Article

Eutectic salt-assisted planetary centrifugal deagglomeration for single-crystalline cathode synthesis

In the format provided by the authors and unedited
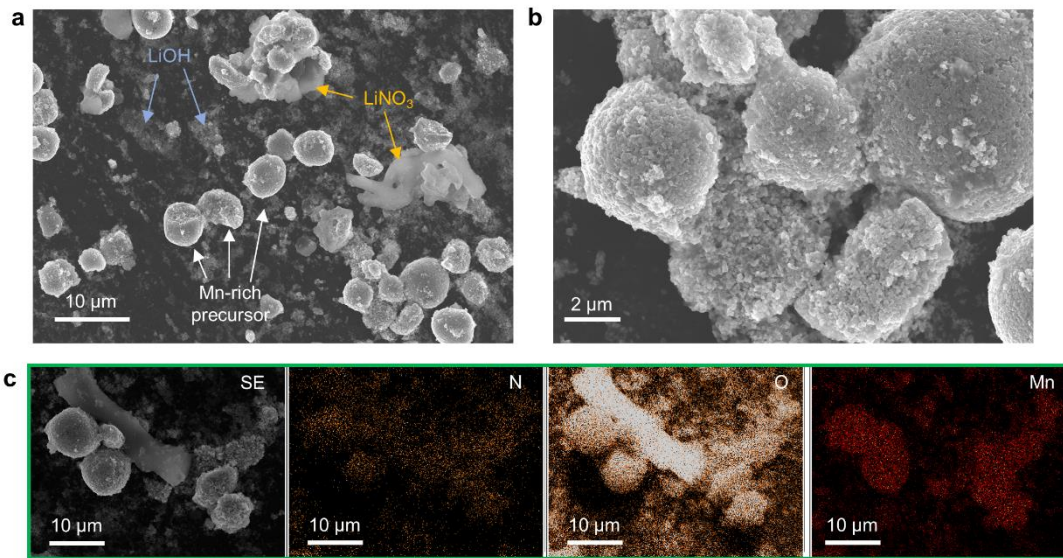
**<u>Table of contents</u>**

Supplementary Figures 1-26

Supplementary Tables 1-9
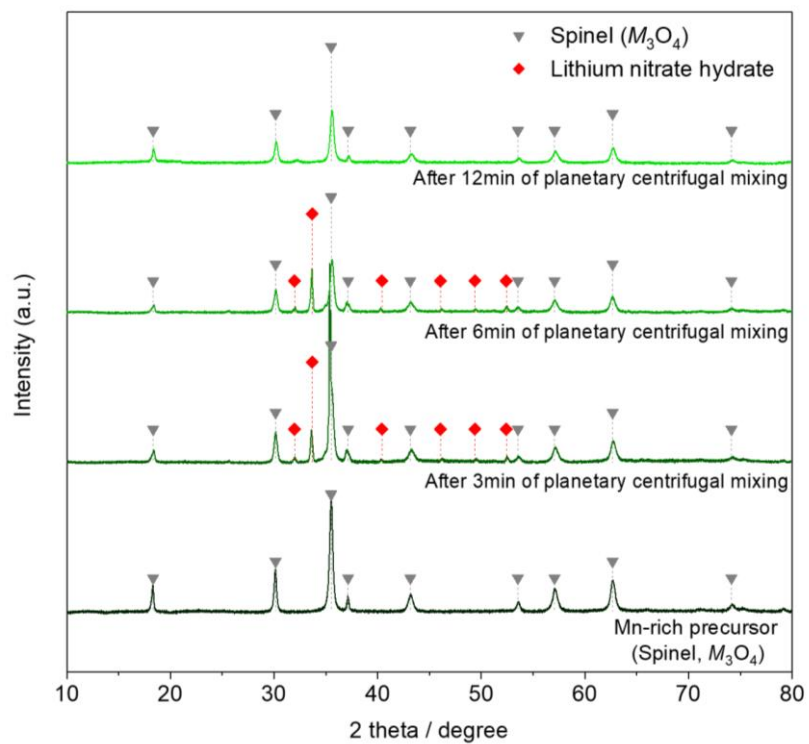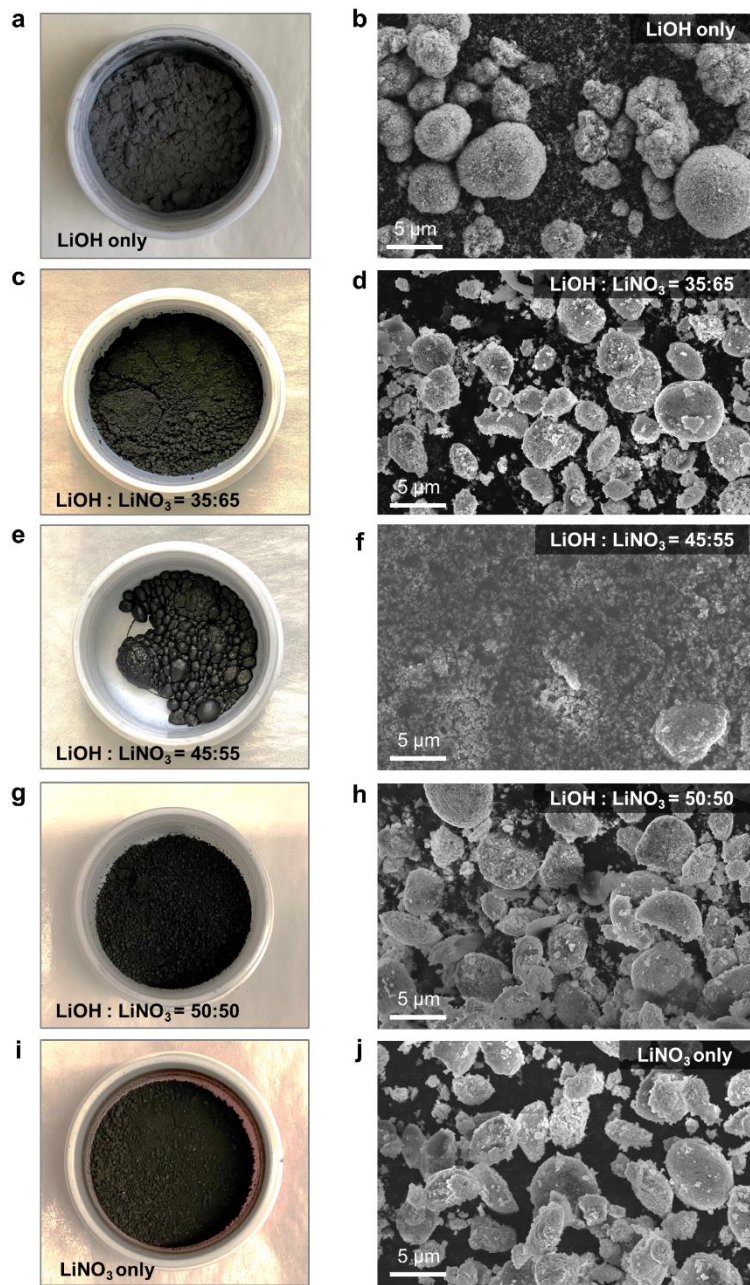
Supplementary Note   1

Supplementary References

Supplementary Figure 1 | Powder mixture of Mn-rich precursor and solid-state Li-based salts (at eutectic composition of LiOH and $LiNO_3$) after 3 min of planetary centrifugal mixing. (a-c) Scanning electron microscopy (SEM) images and energy dispersive spectroscopy (EDS) mapping results of Mn-rich precursor and Li-based salts mixture.
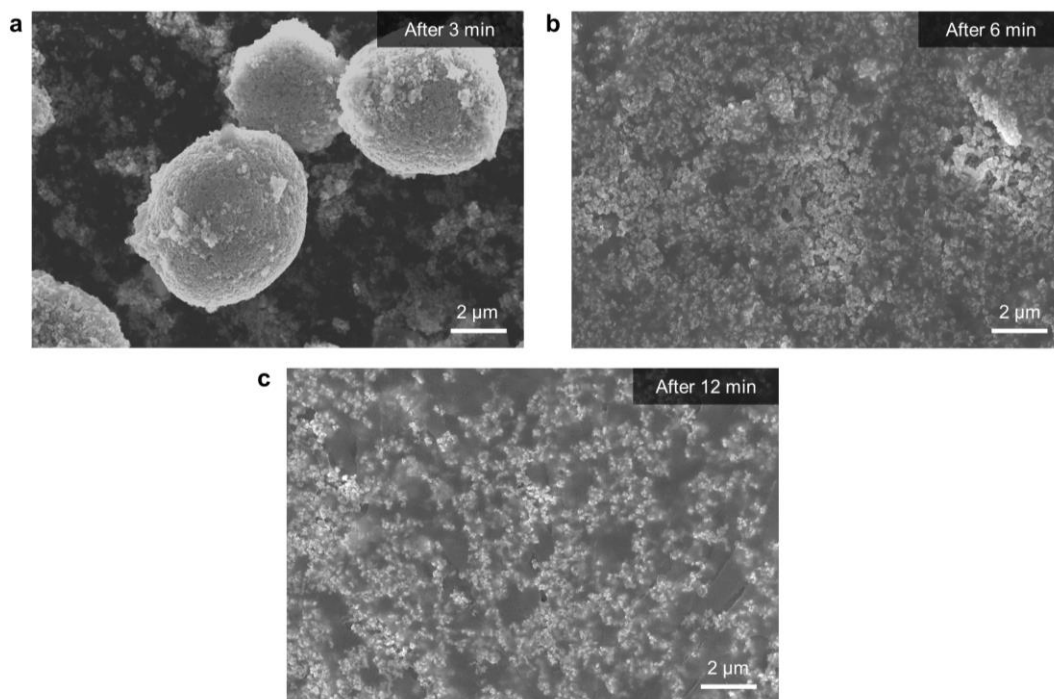
Supplementary Figure 2 | Deagglomeration of secondary particle Mn-rich precursor upon increasing time of planetary centrifugal mixing. (a-c) SEM images of powder mixture of Mn-rich precursor and Li-based solid-/molten-salts (at eutectic composition of LiOH and LiNO$_3$) at each time of planetary centrifugal mixing.

Supplementary Figure 3 | X-ray diffraction (XRD) patterns of powder mixture of Mn-rich precursor and Li-based solid-/molten-salts (at eutectic composition of LiOH and $LiNO_3$) at each time of planetary centrifugal mixing.

Supplementary Figure 4 | Comparison of the effect of particle deagglomeration at different compositions of LiOH-LiNO$_3$ mixture.
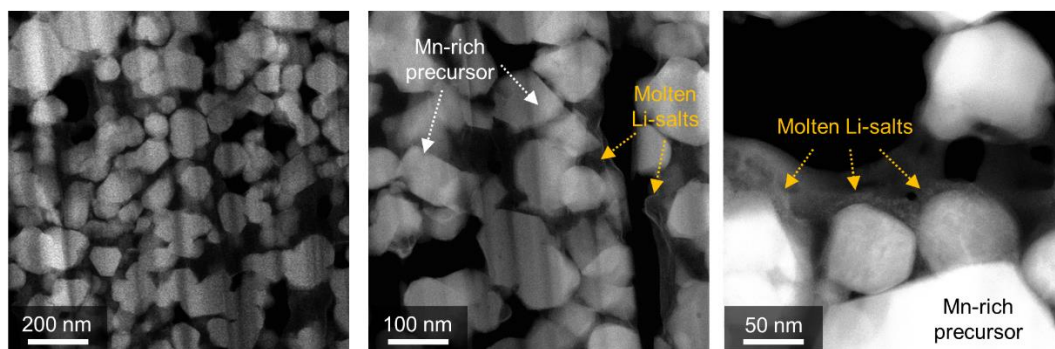
Supplementary Figure 5 | Scanning transmission electron microscopy (STEM) images of cross-sectioned Mn-rich precursor after 12 min of planetary centrifugal deagglomeration. Each primary particle of Mn-rich precursor is distinctly separated by molten Li-salts.
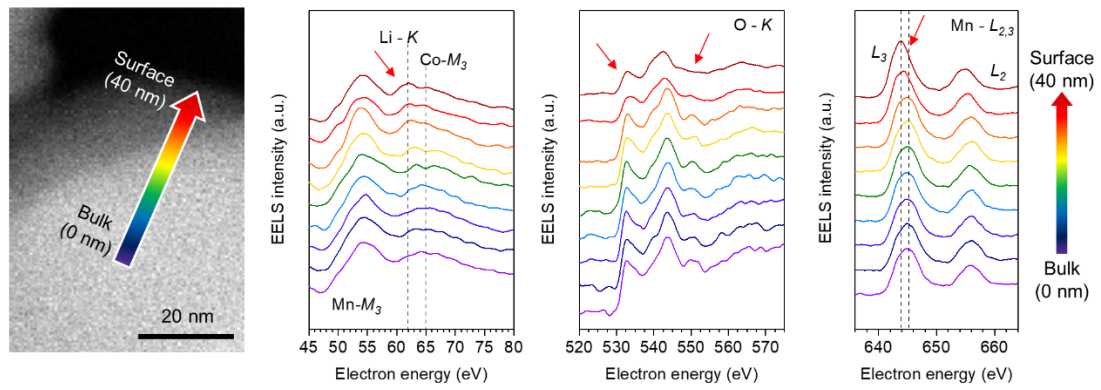
Supplementary Figure 6 | STEM image of Mn-rich precursor and electron energy loss spectroscopy (EELS) line-scanning result along the designated line in selected Mn-rich precursor particle.
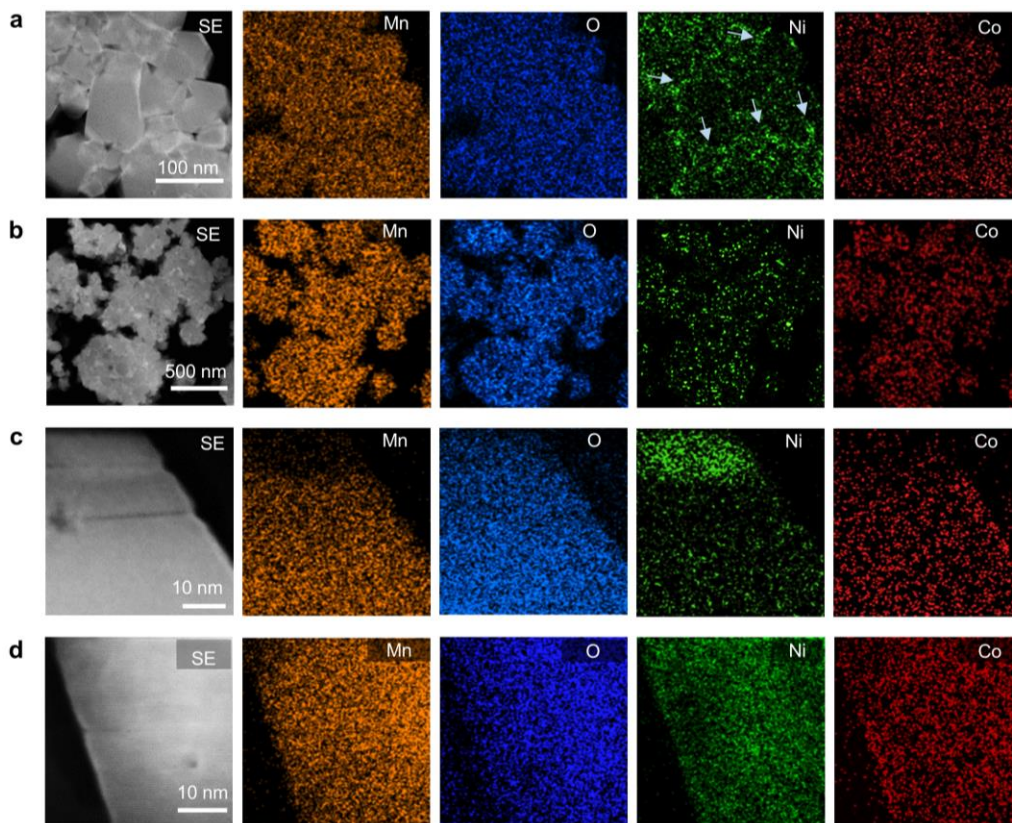
Supplementary Figure 7 | Transmission electron microscopy (TEM)-EDS mapping (Mn, O, Ni, and Co) on cross-sectional particle of (a-c) PC-LMR and (d) SC-LMR.
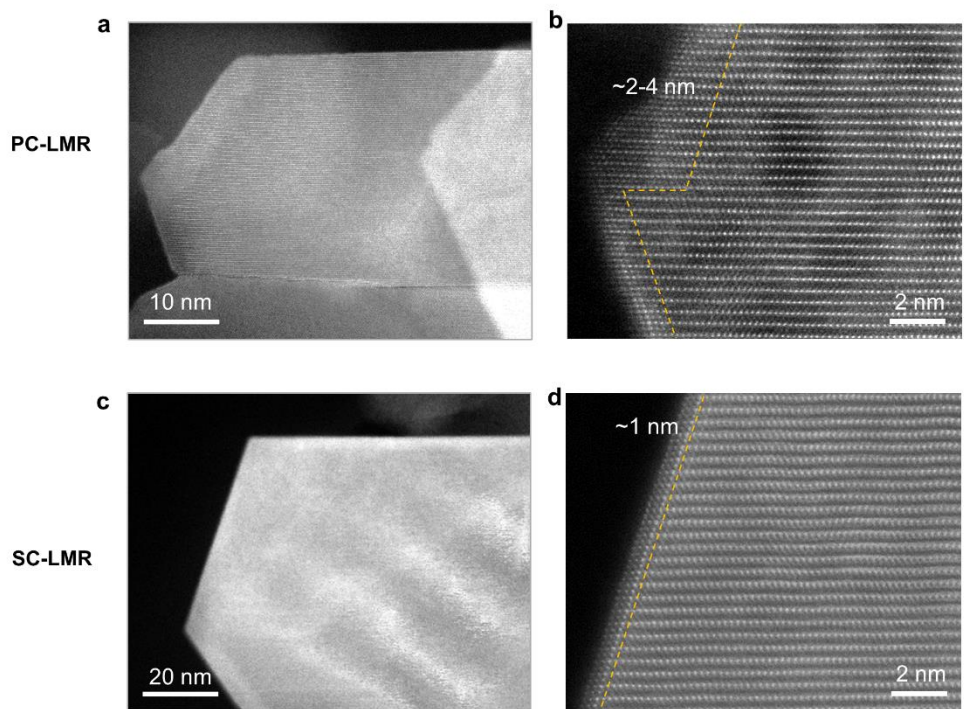
Supplementary Figure 8 | Atomic-resolution STEM images of (a,b) PC-LMR and (c,d) SC-LMR.

PC-LMR has much thicker rock-salt structure along the surface than that of SC-LMR.
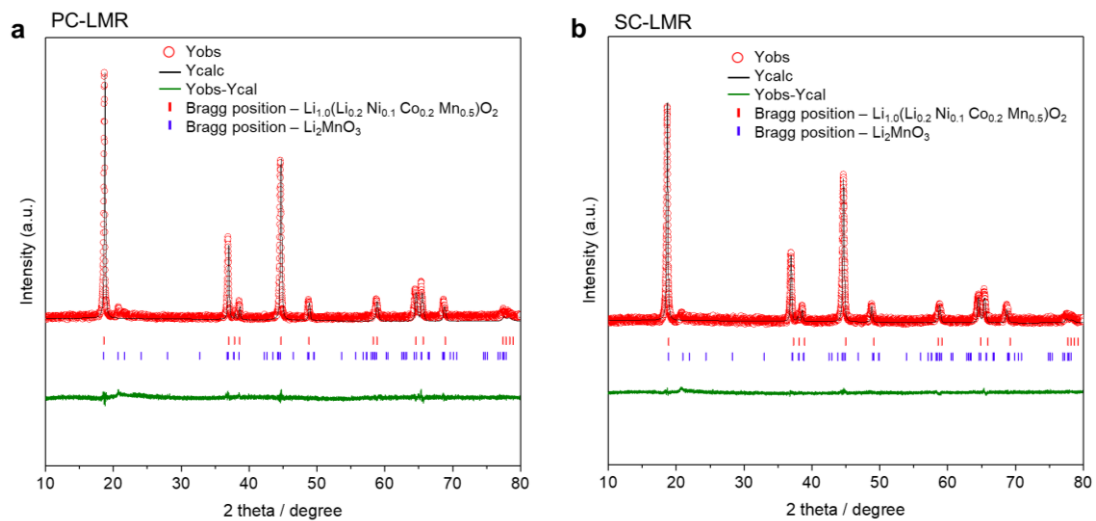
Supplementary Figure 9 | Rietveld refinement of XRD patterns for (a) PC-LMR and (b) SC-LMR.

Fitting details available in Supplementary Table 3.
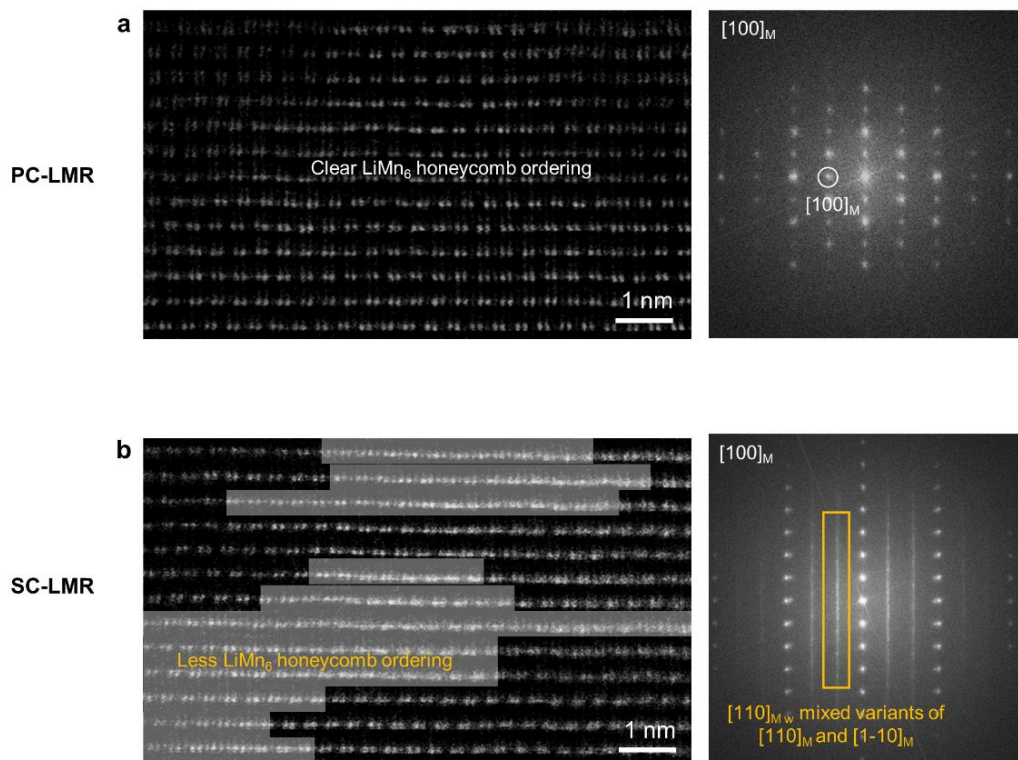
Supplementary Figure 10 | Atomic-resolution STEM images measured along the [100] monoclinic direction. (a) Long-range honeycomb ordering in PC-LMR and (b) short-range honeycomb ordering in SC-LMR and corresponding fast-Fourier transform patterns.
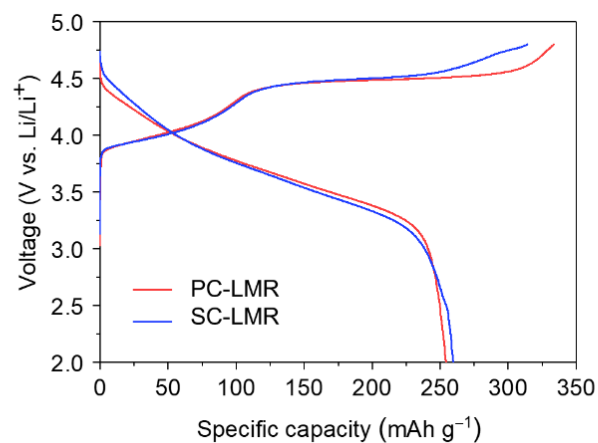
Sample	Charge capacity (mAh g^{-1})	Discharge capacity (mAh g^{-1})	Coulombic efficiency (%)
PC-LMR	333	254	76.2
SC-LMR	314	259	82.4

Supplementary Figure 11 | First-cycle charge-discharge profile (i.e., formation cycle) at 0.1C in between 2.0 and 4.8V (vs. Li/Li$^+$) at 25°C (1C=250 mA g^{-1}).
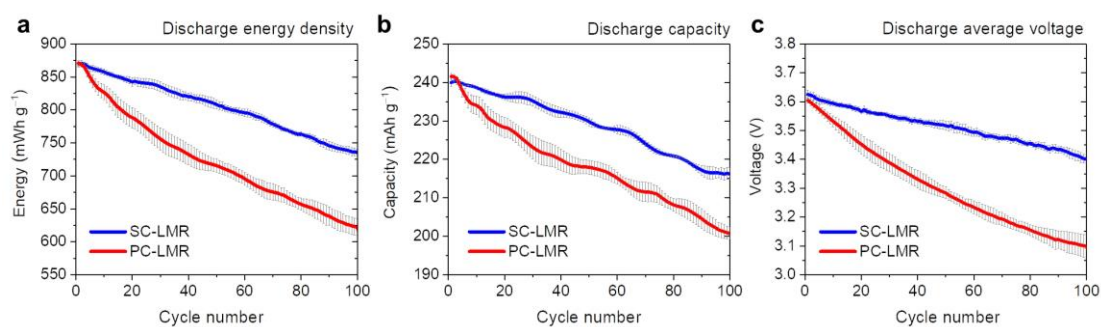
Supplementary Figure 12 | Superior electrochemical performance of SC-LMR over PC-LMR.
(a) Discharge energy density, (b) discharge capacity, and (c) discharge average voltage of PC-LMR and SC-LMR for 100 cycles at 0.3C in the voltage range of 2.0−4.8 V vs. Li/Li$^+$ at 25 ^{o}C (1 C defined as 250 mAh g^{-1}). Solid curve indicates the mean value for 3 cells. Data are presented as mean values ± standard deviations (SD) of each data point.
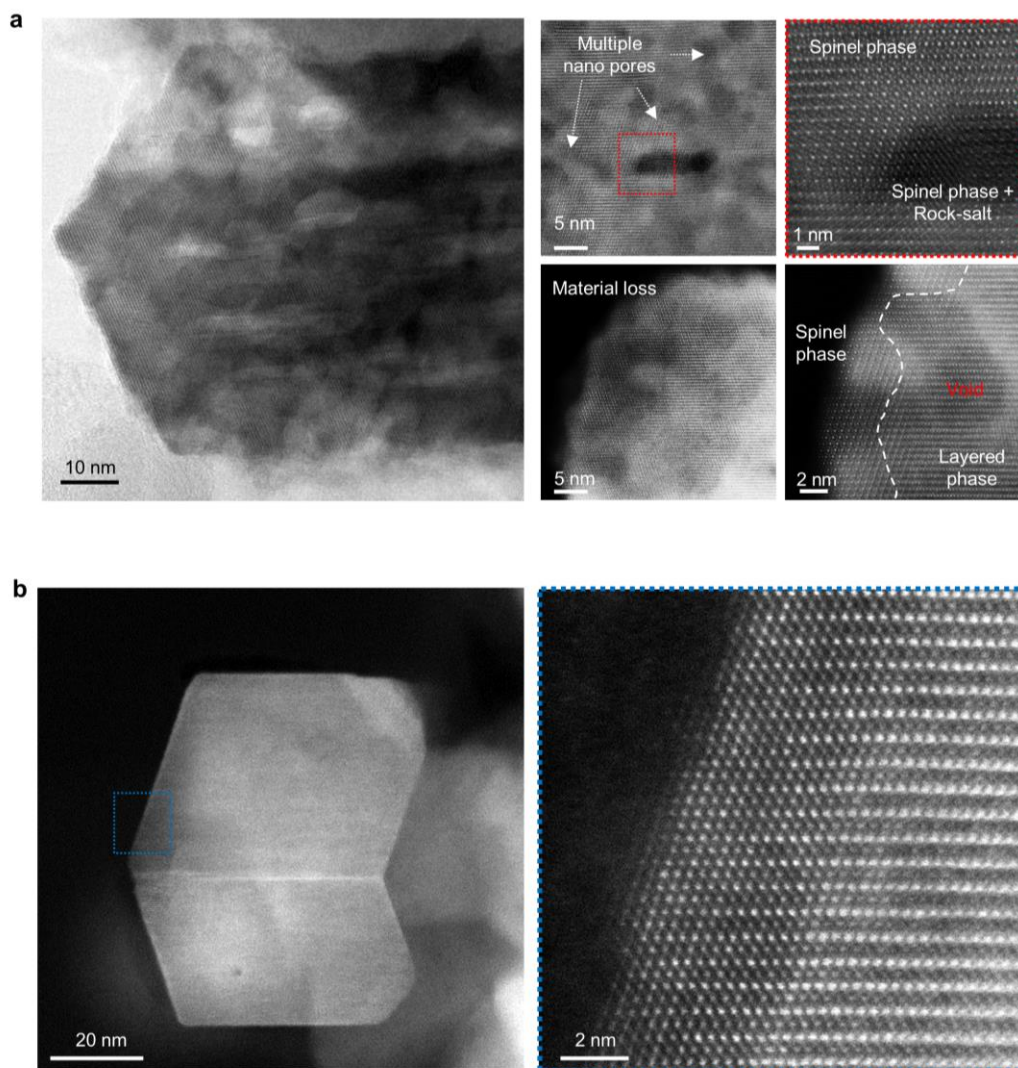
Supplementary Figure 13 | TEM and STEM images of cross-sectioned (a) PC-LMR and (b) SC-LMR after 100 cycles of 0.3C cycling (between 2.0 and 4.8V at 25°C).
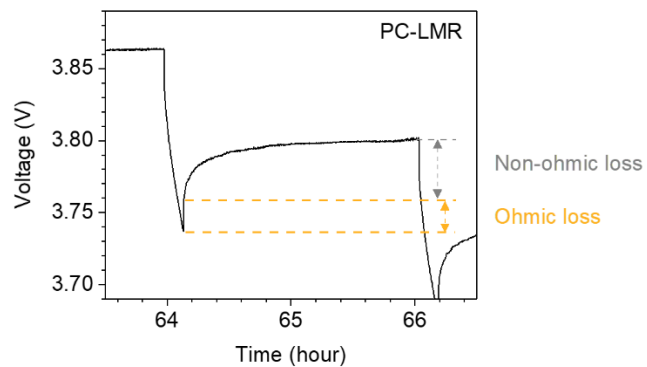
Supplementary Figure 14 | Example showing the measurement of ohmic loss and non-ohmic loss in galvanostatic intermittent titration technique (GITT) curve of PC-LMR after the 5th cycle (between 2.0 and 4.8 V at 25°C).
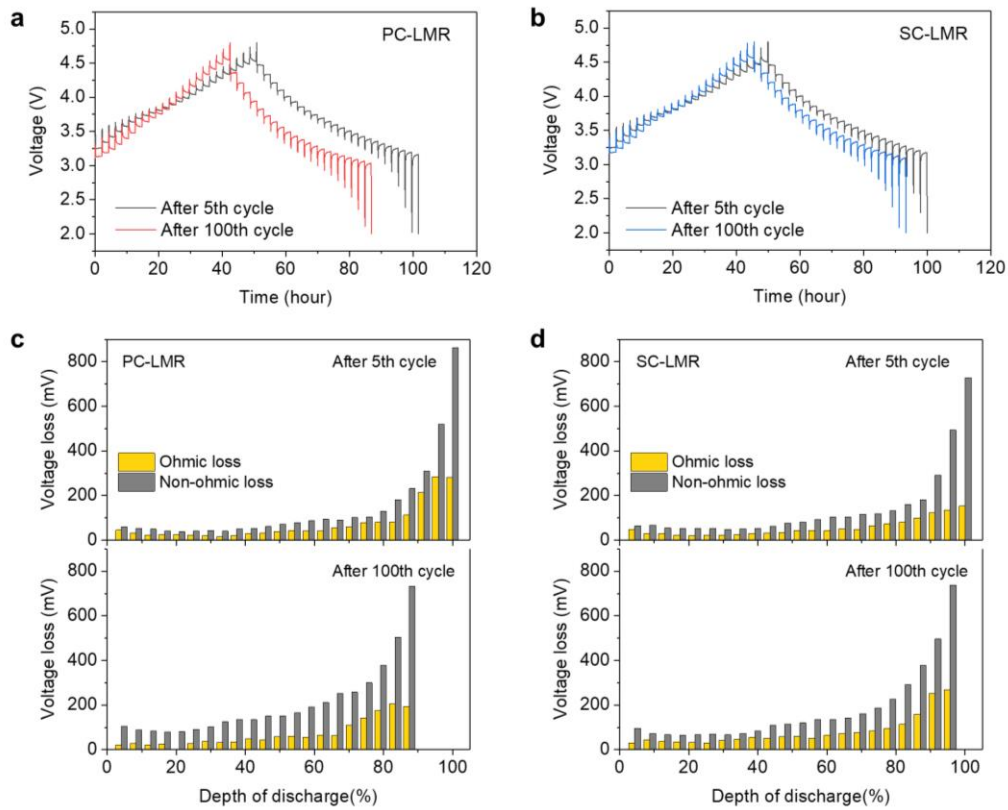
Supplementary Figure 15 | GITT measurements on PC-LMR and SC-LMR after certain cycles of 0.3C cycling (between 2.0 and 4.8V at 25ºC) in **Figure 5c**. The voltage profiles after 5th and 100th cycles for (a) PC-LMR and (b) SC-LMR. The ohmic and non-ohmic voltage losses were separately plotted as a function of depth of discharge in (c) PC-LMR and (d) SC-LMR.
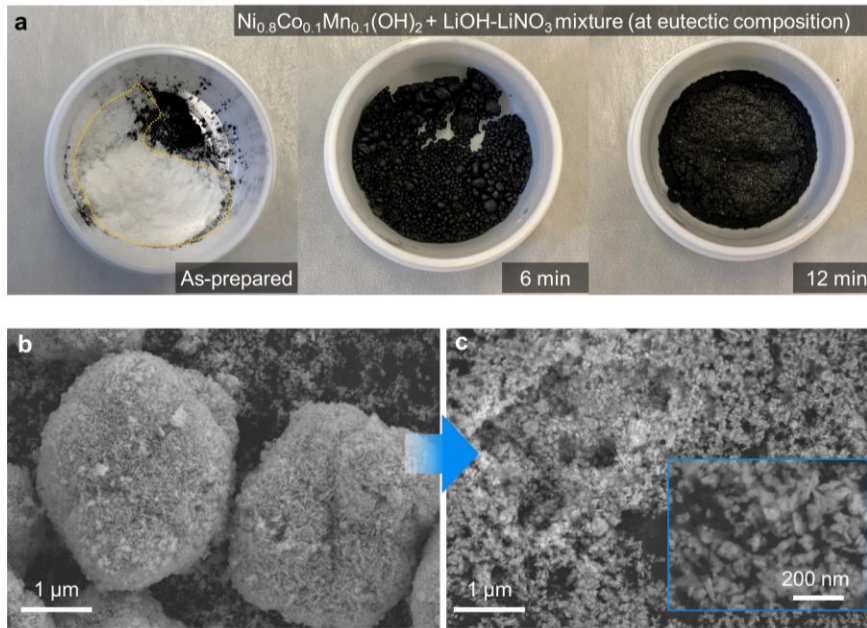
Supplementary Figure 16 | (a) Digital images of Ni-rich precursor ($Ni_{0.8}Co_{0.1}Mn_{0.1}(OH)_2$) and Li-based salts (at eutectic composition of LiOH and $LiNO_3$) mixture at different time of planetary centrifugal mixing (0, 6 and 12min). SEM images of powder mixture (b) after 3 min and (c) 12 min of mixing.
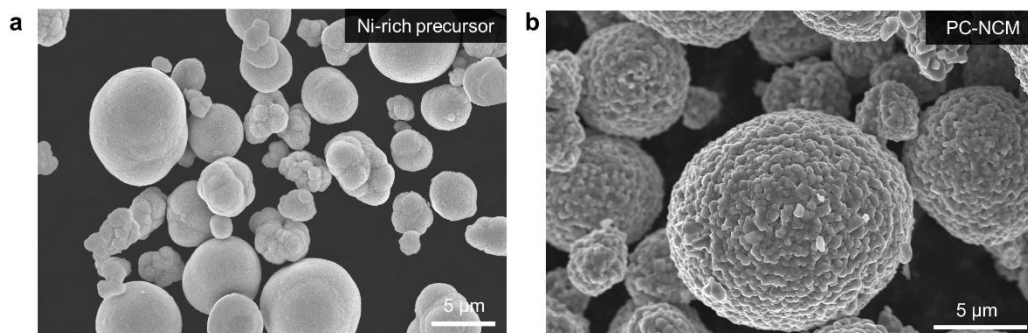
Supplementary Figure 17 | SEM images of (a) Ni-rich precursor ($Ni_{0.8}Co_{0.1}Mn_{0.1}(OH)_2$) and (b) poly-crystalline NCM (PC-NCM) particles.
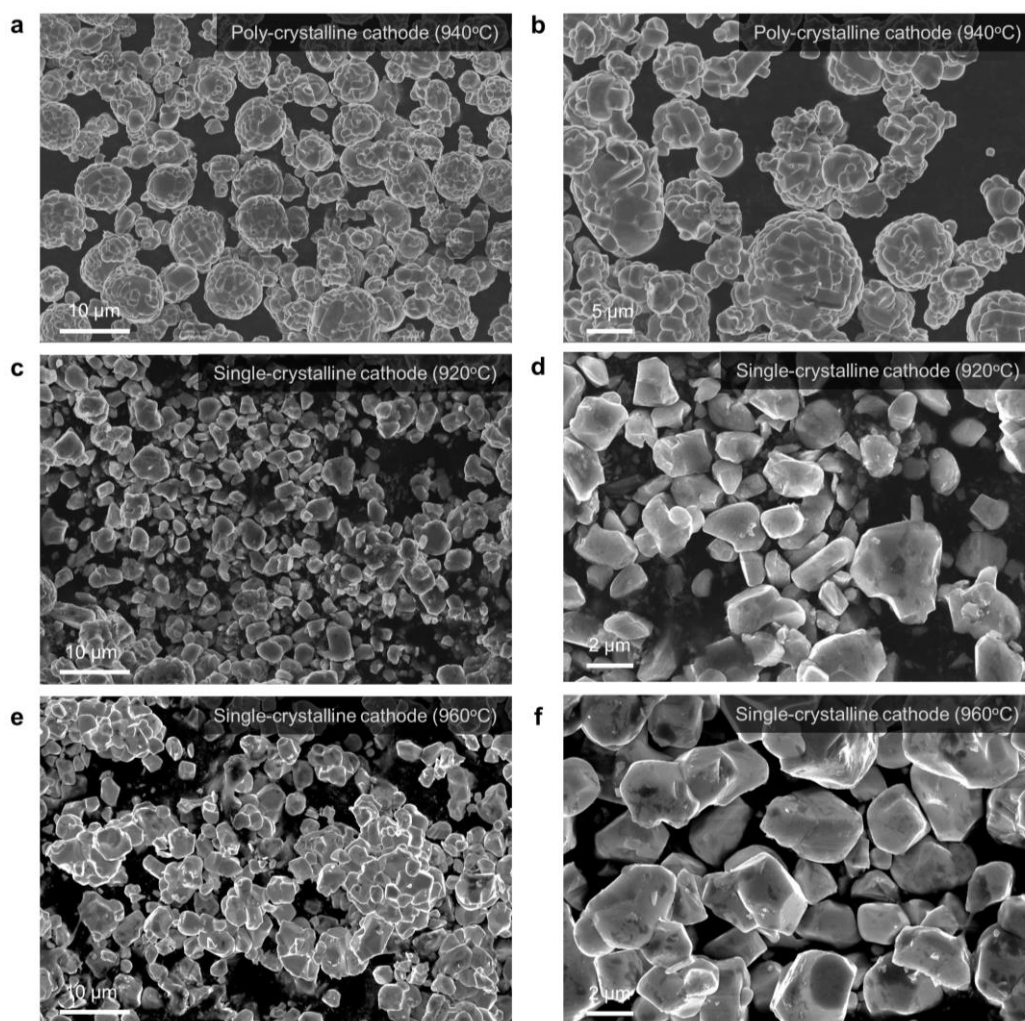
Supplementary Figure 18 | NCM synthesized by eutectic LiOH-LiNO$_3$ mixture with hand-mixing and calcined at 940°C for 2 h and then at 760°C for 10 h in flowing oxygen (a,b), and Ni-rich cathode synthesized by eutectic LiOH-LiNO$_3$ mixture with planetary centrifugal mixing and calcined at 920°C for 2 h and then at 760°C for 10 h (c,d), and 960°C for 2 h and then at 760°C for 10 h (e,f) in flowing oxygen.
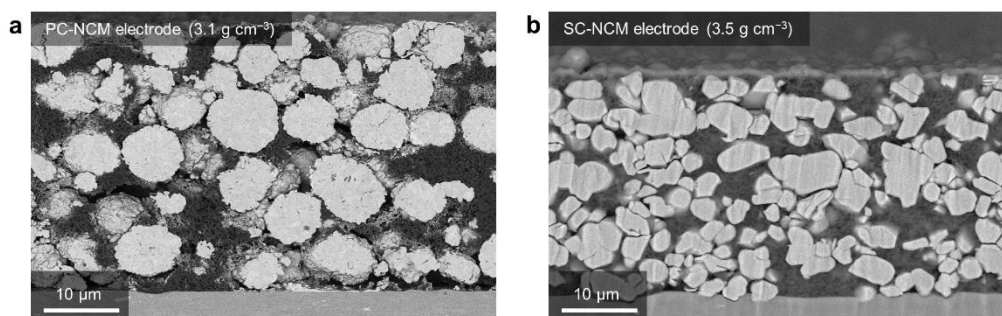
Supplementary Figure 19 | SEM images of cross-sectioned (a) PC-NCM and (b) single-crystalline

NCM (SC-NCM) electrodes before cycling.
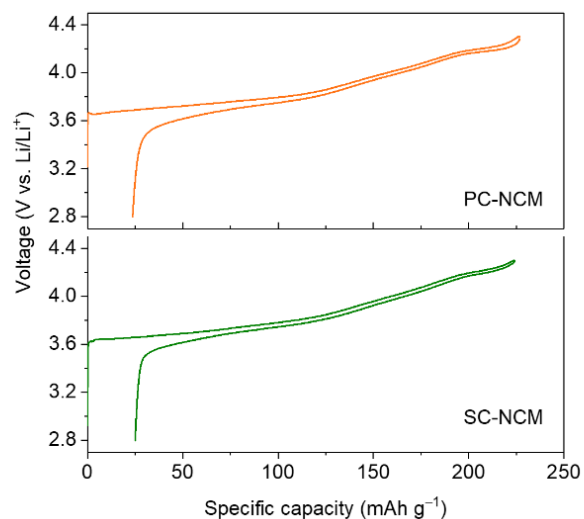
Sample	Charge capacity (mAh g^{-1})	Discharge capacity (mAh g^{-1})	Coulombic efficiency (%)
PC-NCM	226	203	89.8
SC-NCM	224	199	88.8

Supplementary Figure 20 | First-cycle charge-discharge profile (i.e., formation cycle) at 0.1 C in between 2.8 and 4.3 V (vs. Li/Li$^+$) at 25°C (1 C=200 mA g^{-1}).
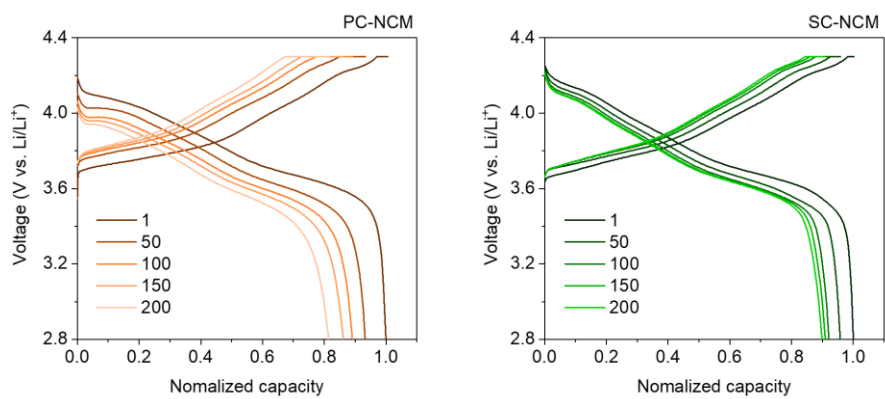
Supplementary Figure 21 | Voltage profiles of PC-NCM and SC-NCM during 0.5 C/0.5 C cycling test in Figure 6e between 2.8 and 4.3 V (vs. Li/Li$^+$) at 25°C (1 C=200 mA g^{-1}).
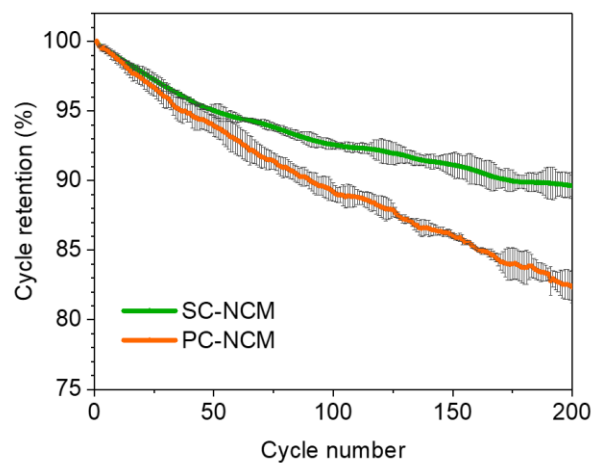
Supplementary Figure 22 | Cycling performance of SC-NCM and PC-NCM for 200 cycles at 0.5 C/0.5 C charge/discharge rate in the voltage range of 2.8−4.3 V vs. Li/Li$^+$ at 25 ℃ (1 C defined as 200 mAh g^{-1}). Solid curve indicates the mean value for 3 cells. Data are presented as mean values ± SD of each data point.
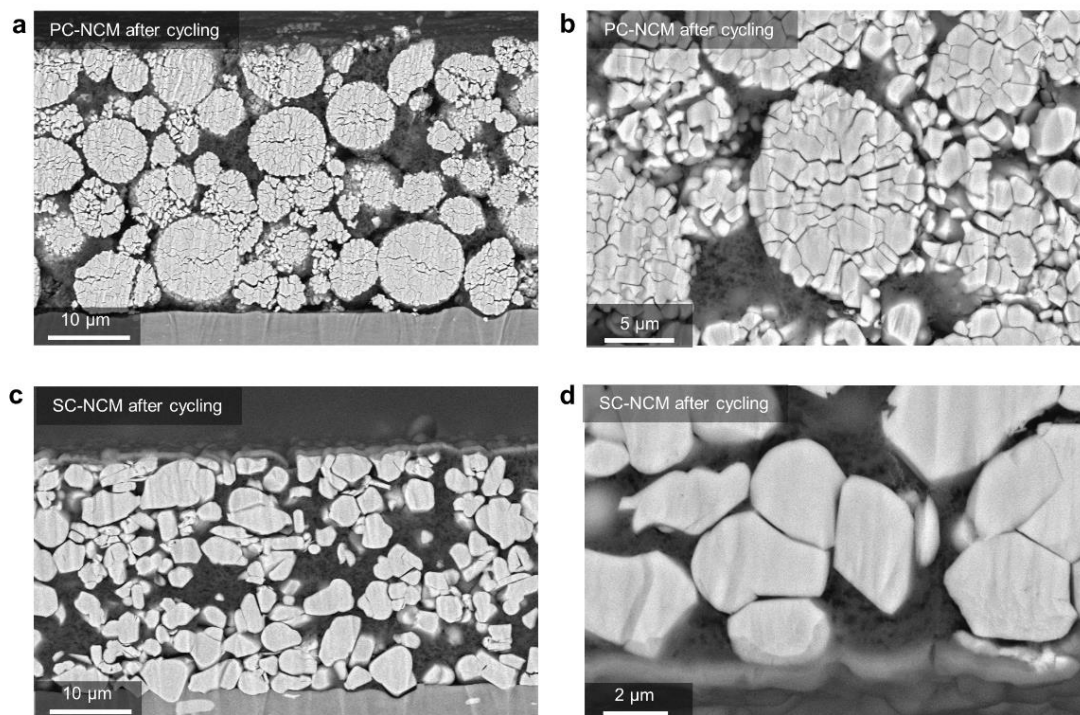
Supplementary Figure 23 | SEM images of cross-sectioned (a,b) PC-NCM and (c,d) SC-NCM electrodes after 200 cycles at 0.5 C/0.5 C within voltage of 2.8-4.3 V (vs. Li/Li$^+$)

a PC-NCM

	PC-NCM	
Sample	5 cycles	200 cycles
R_s (Ω)	2.2	13.1
R_{film} (Ω)	42.8	74.8
R_{CT} (Ω)	71.4	322.4

b SC-NCM

	SC-NCM	
Sample	5 cycles	200 cycles
R_s (Ω)	3.0	5.5
R_{film} (Ω)	16.4	31.2
R_{CT} (Ω)	78.1	182.7
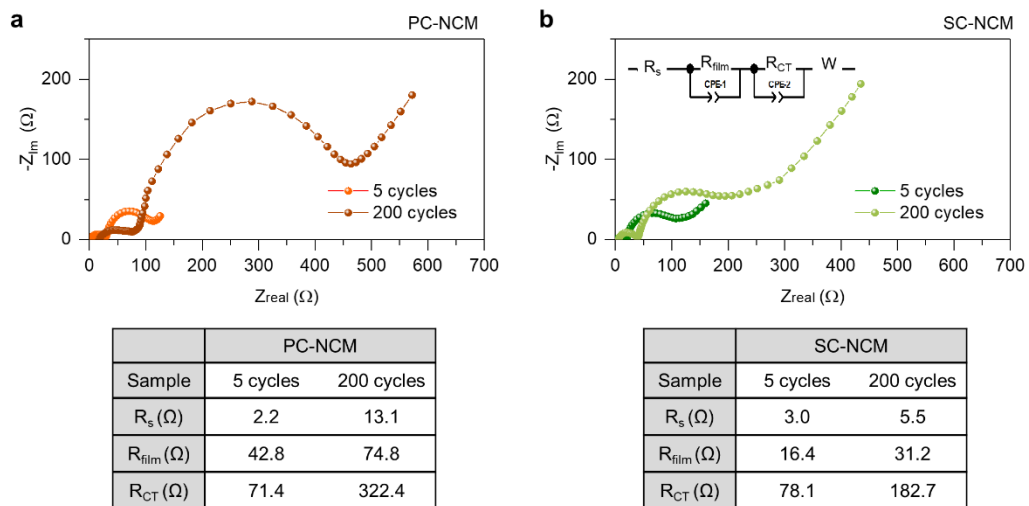
Supplementary Figure 24 | Electrochemical impedance spectroscopy (EIS) measurements on (a) PC-NCM and (b) SC-NCM after 5 and 200 cycles of 0.5 C/0.5 C cycling between 2.8 V and 4.3 V (vs. Li/Li$^+$) at 25°C.
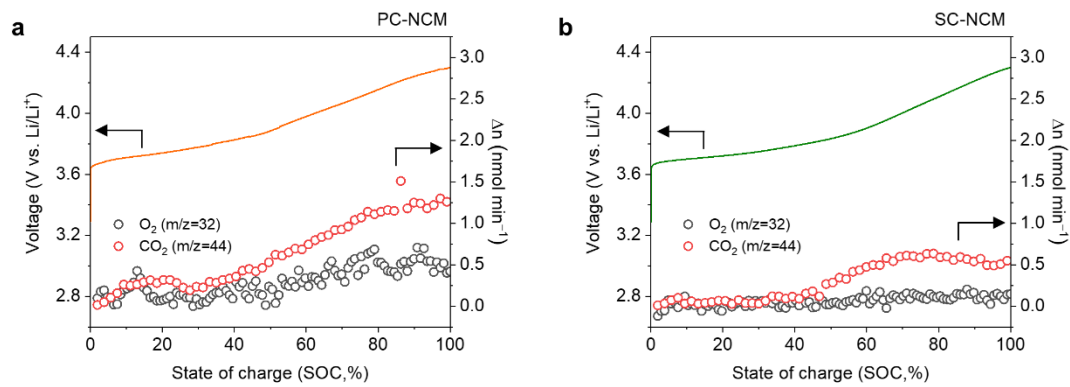
Supplementary Figure 25| In-situ differential electrochemical mass spectrometry data of (a) PC-NCM and (b) SC-NCM during first charge at 0.05 C in the voltage range of 2.8−4.3 V (vs. Li/Li$^+$) at 25°C.
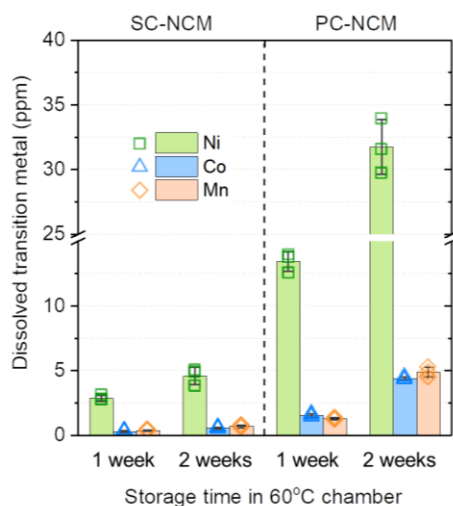
SC-NCM	after 1 week			after 2 weeks		
	Ni (ppm)	Co (ppm)	Mn (ppm)	Ni (ppm)	Co (ppm)	Mn (ppm)
1st batch	2.72	0.31	0.39	3.82	0.51	0.59
2nd batch	2.77	0.36	0.44	5.06	0.59	0.77
3rd batch	3.11	0.26	0.34	4.88	0.65	0.77
Mean	2.87	0.31	0.39	4.59	0.58	0.71
SD	±0.21	±0.05	±0.05	±0.67	±0.07	±0.10

PC-NCM	after 1 week			after 2 weeks		
	Ni (ppm)	Co (ppm)	Mn (ppm)	Ni (ppm)	Co (ppm)	Mn (ppm)
1st batch	13.77	1.68	1.22	31.57	4.33	4.5
2nd batch	13.96	1.57	1.38	29.73	4.31	4.88
3rd batch	12.56	1.44	1.26	33.93	4.53	5.26
Mean	13.43	1.56	1.29	31.74	4.39	4.88
SD	±0.76	±0.12	±0.08	±2.11	±0.12	±0.38

Supplementary Figure 26 | Concentration of dissolved Ni, Co and Mn in electrolytes measured by Inductively coupled plasma - optical emission spectroscopy (ICP-OES), for charged PC-NCM and SC-NCM electrodes during high-temperature storage at 60°C. For each measurement, electrolyte from three batches was analyzed to calculate the mean value and SD. Error bars are presented as ± SD.

Supplementary Table 1 | Chemical composition of PC-LMR and SC-LMR measured by ICP-OES.

Sample	Mole ratio over (Ni+Co+Mn) (%)			
	Li	Ni	Co	Mn
PC-LMR	149.2	20.03	20.15	59.82
SC-LMR	148.5	19.99	20.14	59.86

Supplementary Table 2 | Particle size distributions of PC-LMR and SC-LMR.

Sample	BET surface area $(m^2\,g^{-1})$	Particle size distribution		
		D_{10} (μm)	D_{50} (μm)	D_{90} (μm)
PC-LMR	1.3862	5.7	10.7	22.3
SC-LMR	0.824	1.3	3.75	10.2

Supplementary Table 3 | Refined XRD data for PC-LMR and SC-LMR assuming Ni and Mn can cation-mixed with Li.

PC-LMR	Element	x	y	z	Occupancy
	Li (1)	0.000000	0.000000	0.000000	0.977
R-3m phase a=2.8512 Å c=14.2297Å	O (1)	0.000000	0.000000	0.24117(6)	1.000
	Co (1)	0.000000	0.000000	0.500000	0.160
C2/m phase a=4.9485 Å b=8.5462 Å c=5.0358 Å	Ni (1)	0.000000	0.000000	0.500000	0.142
	Mn (1)	0.000000	0.000000	0.500000	0.475
R_{wp} = 2.73% R_p = 2.11% χ^2= 2.493 S = 1.578	Li (2)	0.000000	0.000000	0.500000	0.223
	Ni (2)	0.000000	0.000000	0.000000	0.018
	Mn (2)	0.000000	0.000000	0.000000	0.005

SC-LMR	Element	x	y	z	Occupancy
	Li (1)	0.000000	0.000000	0.000000	0.961
R-3m phase a=2.8519 Å c=14.2331Å	O (1)	0.000000	0.000000	0.24117(6)	1.000
	Co (1)	0.000000	0.000000	0.500000	0.160
C2/m phase a=4.9489 Å b=8.5485 Å c=5.0364 Å	Ni (1)	0.000000	0.000000	0.500000	0.133
	Mn (1)	0.000000	0.000000	0.500000	0.468
R_{wp} = 2.77% R_p = 2.07% χ^2= 2.590 S = 1.609	Li (2)	0.000000	0.000000	0.500000	0.239
	Ni (2)	0.000000	0.000000	0.000000	0.027
	Mn (2)	0.000000	0.000000	0.000000	0.012

Supplementary Table 4 | Comparison of different Li-/Mn-rich cathode materials on the synthesis method, cost, test specification and electrochemical performances.

Active material	Synthesis method	Li-salt[*] (cost per gram)	Voltage range (vs. Li/Li$^+$)	Initial capacity (energy density)	Capacity retention (energy retention)	Electrode information
DS-LMR (Ref. 1) ($Li_{1.11}Mn_{0.49}Ni_{0.29}Co_{0.11}O_2$) Partice size:700-800 nm	Co-precipitation Ball-milling Solid-state method	Li_2CO_3 ($0.356)	2.0-4.6V	240 mAh g^{-1} (2880 Wh L^{-1})	Not provided (~67.2%) after 100 cycles (0.16C[**])	▪ 10 mg cm^{-2} ▪ 90% AM[***]
SC-LLNMO (Ref. 2) ($Li_{1.2}Ni_{0.2}Mn_{0.6}O_2$) Partice size:300-600 nm	Co-precipitation Molten-salt method (Li_2CO_3-LiCl) Washing	Li_2CO_3-LiCl ($0.407)	2.0-4.8V	257 mAh g^{-1} (Not provided)	92% (not provided) after 200 cycles (1.0C)	▪ Not provided ▪ 70% AM
SC-LMR (our work) ($Li_{1.2}Mn_{0.48}Ni_{0.16}Co_{0.16}O_2$) Partice size: ~1 μm	Co-precipitation Molten-salt method (LiOH-LiNO$_3$)	LiOH-LiNO$_3$ ($0.321)	2.0-4.8V	259 mAh g^{-1} (2922Wh L^{-1})	90.6% (~84.9%) after 100 cycles (0.3C)	▪ 10 mg cm^{-2} ▪ 90% AM

*Based on price from Sigma-Aldrich   **1.0C = 250 mA g^{-1} ***AM : Active material

Supplementary Table 5 | Concentration of dissolved Ni, Co and Mn in electrolytes measured by ICP-OES, for charged PC-LMR and SC-LMR electrodes during high-temperature storage at 60°C. For each measurement, electrolyte from three batches was analyzed to calculate the mean value and SD.

PC-LMR	after 1 week			after 2 weeks		
	Ni (ppm)	Co (ppm)	Mn (ppm)	Ni (ppm)	Co (ppm)	Mn (ppm)
1st batch	8.36	3.55	24.08	14.39	8.76	63.88
2nd batch	8.49	3.82	25.44	16.62	8.64	66.41
3rd batch	8.25	3.98	25.46	18.42	8.53	68.06
Mean	8.37	3.78	24.99	16.48	8.64	66.12
SD	±0.12	±0.22	±0.79	±2.02	±0.12	±2.11
SC-LMR	**after 1 week**			**after 2 weeks**		
	Ni (ppm)	Co (ppm)	Mn (ppm)	Ni (ppm)	Co (ppm)	Mn (ppm)
1st batch	1.94	1.2	6.08	4.63	2.72	10.85
2nd batch	2.04	1.11	5.91	4.87	2.55	10.86
3rd batch	2.14	1.3	5.65	4.66	2.77	9.7
Mean	2.04	1.20	5.88	4.72	2.68	10.47
SD	±0.10	±0.10	±0.22	±0.13	±0.12	±0.67

Supplementary Table 6 | Chemical composition of PC-NCM and SC-NCM measured by ICP-OES.

Sample	Mole ratio over (Ni+Co+Mn) (%)			
	Li	Ni	Co	Mn
PC-NCM	101.4	79.754	10.347	9.899
SC-NCM	101.8	79.847	10.256	9.897

Supplementary Table 7 | Particle size distributions of PC-NCM and SC-NCM

Sample	BET surface area (m^2 g^{-1})	Particle size distribution		
		D_{10} (µm)	D_{50} (µm)	D_{90} (µm)
PC-NCM	0.5278	6.7	13.6	24.7
SC-NCM	0.2389	2.2	4.8	12.7

Supplementary Table 8 | Refined XRD data for PC-NCM and SC-NCM assuming only Ni can do cation-mixing with Li.

PC-NCM	Element	Site	x	y	z	Occupancy
	Li	3a	0	0	0	0.991(6)
a=2.86034(3) Å	Li	3b	0	0	0.5	0.009(7)
c=14.24706(5) Å	Co	3b	0	0	0.5	0.102(4)
R_{wp} = 3.79%	Ni	3b	0	0	0.5	0.790(3)
R_p = 2.85%	Mn	3b	0	0	0.5	0.099(6)
χ^2= 2.40	Ni	3a	0	0	0	0.009(6)
S = 1.55	O	6c	0	0	0.259643	1.0(4)

SC-NCM	Element	Site	x	y	z	Occupancy
	Li	3a	0	0	0	0.989(6)
a=2.86385(3) Å	Li	3b	0	0	0.5	0.011(6)
c=14.22471(6) Å	Co	3b	0	0	0.5	0.102(4)
R_{wp} = 3.81%	Ni	3b	0	0	0.5	0.788(4)
R_p = 2.87%	Mn	3b	0	0	0.5	0.099(4)
χ^2= 2.22	Ni	3a	0	0	0	0.011(6)
S = 1.49	O	6c	0	0	0.256735	1.0(4)

Supplementary Table 9 | Comparison of single-crystalline Ni-rich cathode materials on the synthesis method, particle size, and electrochemical performances.

Active material	Synthesis method	Particle size	Voltage range (vs. Li/Li$^+$)	Discharge capacity @ 1st cycle (mAh g^{-1})	Capacity retention	Electrode loading and AM* ratio
$Li_{1.0}Ni_{0.8}Co_{0.1}Mn_{0.1}O_2$ (Ref. 3)	Commercial (Not provided)	2-3μm	3.0-4.3V	180	79.6% after 200 cycles (0.1C)	• 10 mg cm^{-2} • 80% AM
$Li_{1.0}Ni_{0.8}Co_{0.1}Mn_{0.1}O_2$ (Ref. 4)	Co-precipitation High-temperature synthesis (multi-step)	2-3μm	2.5-4.4V	210	92.6% after 100 cycles (0.33C)	• 3 mg cm^{-2} • 80% AM
$Li_{1.0}Ni_{0.8}Co_{0.1}Mn_{0.1}O_2$ (Ref. 5)	CATL (China)	2-3μm	2.8-4.3V	195	90.9% after 50 cycles (0.2C)	• 10 mg cm^{-2} • 80% AM
$Li_{1.0}Ni_{0.6}Co_{0.2}Mn_{0.2}O_2$ (Ref. 6)	Commercial (Not provided)	2-3μm	3.0-4.3V	152	76.9% after 200 cycles (1.0C)	• 2-3 mg cm^{-2} • 80% AM
$Li_{1.0}Ni_{0.8}Co_{0.1}Mn_{0.1}O_2$ (Ref. 7)	Commercial (Not provided)	2-3μm	2.8-4.3V	170	77.7% after 200 cycles (1.0C)	• 4.8 mg cm^{-2} • 85% AM
$Li_{1.0}Ni_{0.8}Co_{0.1}Mn_{0.1}O_2$ (Ref. 8)	Commercial (Singular Materials Lab. Co., Korea)	2-3μm	3.0-4.3V	192	89.0% after 100 cycles (1.0C)	• 26.4 mg cm^{-2} • 96% AM
$Li_{1.0}Ni_{0.8}Co_{0.1}Mn_{0.1}O_2$ (Ref. 9)	Commercial (Beijing IA Metal New Energy Co. ,China)	2-3μm	3.0-4.3V	175	86.7% after 100 cycles (0.5C)	• 3.5 mg cm^{-2} • 90% AM
$Li_{1.0}Ni_{0.8}Co_{0.1}Mn_{0.1}O_2$ (Ref. 10)	Spray pyrolysis High-temperature synthesis (multi-step)	~1μm	3.0-4.4V	174	68.2% after 100 cycles (1.0C)	• Not provided
$Li_{1.0}Ni_{0.83}Co_{0.11}Mn_{0.06}O_2$ (Ref. 11)	Molten-salt method (Not provided)	0.5-2μm	2.7-4.3V	177	92.8% after 100 cycles (1.0C)	• Not provided
$Li_{1.0}Ni_{0.8}Co_{0.1}Mn_{0.1}O_2$ (Ref. 12)	Co-precipitation High-temperature synthesis (one-step)	2-3μm	2.7-4.3V	186	85.0% after 100 cycles (0.5C)	• 4-5 mg cm^{-2} • 90% AM
$Li_{1.0}Ni_{0.8}Co_{0.1}Mn_{0.1}O_2$ (Ref. 13)	Co-precipitation High-temperature synthesis (one-step)	2-3μm	2.8-4.3V	160	86.3% after 200 cycles (1.0C)	• 2-3 mg cm^{-2} • 80% AM
$Li_{1.0}Ni_{0.8}Co_{0.1}Mn_{0.1}O_2$ (Ref. 14)	Commercial (Hunan Changyuan Lico Co., China)	3-6μm	2.8-4.3V	184	86.5% after 200 cycles (1.0C)	• 3.75mg cm^{-2} • 80% AM
$Li_{1.0}Ni_{0.88}Co_{0.09}Al_{0.03}O_2$ (Ref. 15)	Co-precipitation High-temperature synthesis (multi-step)	3-6μm	3.0-4.3V	185	85.0% after 100 cycles (0.2C)	• 12 mg cm^{-2} • 92% AM
$Li_{1.0}Ni_{0.6}Co_{0.2}Mn_{0.2}O_2$ (Ref. 16)	Co-precipitation High-temperature synthesis (multi-step) Grinding	1-4 um	3.0-4.4V	168	84-90% after 50 cycles (0.2C)	• 12 mg cm^{-2} • 92% AM
$Li_{1.0}Ni_{0.8}Co_{0.1}Mn_{0.1}O_2$ (Ref. 17)	Commercial (Beijing IA Metal New Energy Co. ,China)	~3um	3.0-4.3V	180	77.4% after 200 cycles (0.5C)	• 7 mg cm^{-2} • 90% AM
$Li_{1.0}Ni_{0.83}Co_{0.11}Mn_{0.06}O_2$ (Ref. 18)	Co-precipitation High-temperature synthesis (multi-step)	1-4 um	2.75-4.4V	191	84.5% after 150 cycles (1.0C)	• 8.5 mg cm^{-2} • 89% AM
$Li_{1.0}Ni_{0.8}Co_{0.1}Mn_{0.1}O_2$ (Ref. 19)	Co-precipitation High-temperature synthesis (one-step)	2-5um	2.8-4.5V	190	58.7% after 400 cycles (1.0C)	• 4 mg cm^{-2} • 80% AM
$Li_{1.0}Ni_{0.8}Co_{0.1}Mn_{0.1}O_2$ (Our work)	LiOH-LiNO$_3$ Molten-salt method	1-4 um	2.8-4.3V	189	89.7% after 200 cycles (0.5C)	• 10 mg cm^{-2} • 90% AM
	LiOH-LiNO$_3$ Molten-salt method	1-4 um	2.8-4.4V	205	92.7% after 100 cycles (0.5C)	• 10 mg cm^{-2} • 90% AM

Supplementary Note 1 | Implications from GITT measurements

For PC-LMR and SC-LMR after the 5th cycle (**Supplementary Figure 15**), the overpotentials (ohmic and non-ohmic parts) are relatively small at all states of charge except the end of discharge (e.g., the last three titration + relaxation steps). Excluding the last three GITT steps (layered cathodes are known to have large overpotential at the end of discharge, i.e., close to the fully lithiated state), the ohmic part of the overpotential is 43.79±25.57 mV for PC-LMR and 43.20±21.71 mV for SC-LMR, and the non-ohmic part is 81.36±49.63 mV for PC-LMR and 86.38±38.60 mV for SC-LMR. The results indicate that despite much larger primary particle size, SC-LMR has good kinetics and similar electrochemical performance to PC-LMR.

The overpotentials of PC-LMR and SC-LMR after the 100th cycle are also plotted in (**Supplementary Figure 15**). Compared to the data after the 5th cycle, there is overpotential growth causing degradations. Excluding the last three GITT steps, the ohmic part of the overpotential is 48.67±33.56 mV for PC-LMR and 50.61±23.02 mV for SC-LMR, and the non-ohmic part is 150.34±67.34 mV for PC-LMR and 120.06±61.45 mV for SC-LMR. The results indicate that the overpotential growth is mainly contributed by the non-ohmic part, which is smaller for SC-LMR than PC-LMR. Since the non-ohmic part can be attributed to Li^+ lattice diffusion within individual particles, it suggests that there are less lattice degradations in SC-LMR than in PC-LMR. For Li-rich layered cathodes with active oxygen redox, lattice cavitation and phase transformation from layered to cation-densified spinel (e.g., Mn_3O_4) phase after electrochemical cycling have been reported in the literature (Ref. 20), which slows down Li^+ lattice diffusion within cathode particles. This is likely the case in our study, where PC-LMR because of smaller primary particle size, electrochemically induced intergranular cracking, and different surface chemistry shows more lattice degradations and side reactions than SC-LMR. The hypothesis is also supported by the DEMS and ICP data, where SC-LMR shows less gas evolution and transition metal dissolution than PC-LMR after electrochemical cycling.

In addition to the above, a key insight from GITT measurements is that SC-LMR shows less degradation in the bulk redox chemistry (inferred from the voltages after each relaxation step, which can be viewed as the voltage profile under the open circuit voltage, OCV, condition) than PC-LMR. The data are plotted as the solid curves in **Figure 5c**. Apparently, there is a large downward shift in the voltage curve of PC-LMR under OCV condition from the 5th to the 100th cycle, while the change is much smaller for SC-LMR. This is consistent with the observation that SC-LMR has less voltage decay than PC-LMR. All these data support the idea that SC-LMR has less bulk degradation than PC-LMR.

Supplementary References

1   Hwang, J. *et al.* Lattice-Oxygen-Stabilized Li- and Mn-Rich Cathodes with Sub-Micrometer Particles by Modifying the Excess-Li Distribution. *Adv. Mater.* **33**, 2100352 (2021).

2   Yang, X. *et al.* Structural Origin of Suppressed Voltage Decay in Single-Crystalline Li-Rich Layered Li[Li$_{0.2}$Ni$_{0.2}$Mn$_{0.6}$]O$_2$ Cathodes. *Small* **18**, 2201522 (2022).

3   Kong, X., Zhang, Y., Peng, S., Zeng, J. & Zhao, J. Superiority of Single-Crystal to Polycrystalline LiNi$_x$Co$_y$Mn$_{1-x-y}$O$_2$ Cathode Materials in Storage Behaviors for Lithium-Ion Batteries. *ACS Sustain. Chem. Eng.* **8**, 14938-14948 (2020).

4   Zhang, R., Wang, C., Ge, M. & Xin, H. L. Accelerated Degradation in a Quasi-Single-Crystalline Layered Oxide Cathode for Lithium-Ion Batteries Caused by Residual Grain Boundaries. *Nano Lett.* **22**, 3818-3824 (2022).

5   Shi, C.-G. *et al.* Investigation and Suppression of Oxygen Release by LiNi$_{0.8}$Co$_{0.1}$Mn$_{0.1}$O$_2$ Cathode under Overcharge Conditions. *Adv. Energy Mater.* **12**, 2200569 (2022).

6   Wang, W. *et al.* Stabilization of a 4.7 V High-Voltage Nickel-Rich Layered Oxide Cathode for Lithium-Ion Batteries through Boron-Based Surface Residual Lithium-Tuned Interface Modification Engineering. *ChemElectroChem* **8**, 2014-2021 (2021).

7   Han, Y., Heng, S., Wang, Y., Qu, Q. & Zheng, H. Anchoring Interfacial Nickel Cations on Single-Crystal LiNi$_{0.8}$Co$_{0.1}$Mn$_{0.1}$O$_2$ Cathode Surface via Controllable Electron Transfer. *ACS Energy Lett.* **5**, 2421-2433 (2020).

8   Cha, H. *et al.* Boosting Reaction Homogeneity in High-Energy Lithium-Ion Battery Cathode Materials. *Adv. Mater.* **32**, 2003040 (2020).

9   Zou, Y.-G. *et al.* Mitigating the Kinetic Hindrance of Single-Crystalline Ni-Rich Cathode via Surface Gradient Penetration of Tantalum. *Angew. Chem. Int. Ed.* **60**, 26535-26539 (2021).

10   Zhu, J. *et al.* Flux-free synthesis of single-crystal LiNi$_{0.8}$Co$_{0.1}$Mn$_{0.1}$O$_2$ boosts its electrochemical performance in lithium batteries. *J. Power Sources* **464**, 228207 (2020).

11   Ni, L. *et al.* Single-Crystalline Ni-Rich layered cathodes with Super-Stable cycling. *Chem. Eng. J.* **431**, 133731 (2022).

12   Ryu, H.-H. *et al.* Capacity Fading Mechanisms in Ni-Rich Single-Crystal NCM Cathodes. *ACS Energy Lett.* **6**, 2726-2734 (2021).

13   Zhang, F. *et al.* Surface regulation enables high stability of single-crystal lithium-ion cathodes at high voltage. *Nat. Commun.* **11**, 3050 (2020).

14   Chen, X., Tang, Y., Fan, C. & Han, S. A highly stabilized single crystalline nickel-rich LiNi$_{0.8}$Co$_{0.1}$Mn$_{0.1}$O$_2$ cathode through a novel surface spinel-phase modification. *Electrochim. Acta* **341**, 136075 (2020).

15   Li, H. *et al.* Synthesis of Single Crystal LiNi$_{0.88}$Co$_{0.09}$Al$_{0.03}$O$_2$ with a Two-Step Lithiation Method. *J. Electrochem. Soc.* **166**, A1956-A1963 (2019).

16   Li, H., Li, J., Ma, X. & Dahn, J. R. Synthesis of Single Crystal LiNi$_{0.6}$Mn$_{0.2}$Co$_{0.2}$O$_2$ with Enhanced Electrochemical Performance for Lithium Ion Batteries. *J. Electrochem. Soc.* **165**, A1038-A1045 (2018).

17   Zou, Y.-G. *et al.* Constructing a stable interfacial phase on single-crystalline Ni-rich cathode via chemical reaction with phosphomolybdic acid. *Nano Energy* **87**, 106172 (2021).

18   Fan, X. *et al.* Crack-free single-crystalline Ni-rich layered NCM cathode enable superior cycling performance of lithium-ion batteries. *Nano Energy* **70**, 104450 (2020).

19   Liu, M. *et al.* Dual Design of the Surface via an Ion Conductor Coating and In Situ Electrochemical Diffusion Enabling a Long Life for a Ni-Rich Cathode. *ACS Appl. Energy Mater.* **5**, 9181-9188 (2022).

20   Yan, P., Zheng, J., Tang, ZK. et al. Injection of oxygen vacancies in the bulk lattice of layered cathodes. *Nat. Nanotechnol.* **14**, 602–608 (2019).